applied optics

Dissolved gas sensing using an anti-resonant hollow core optical fiber

JASON KAPIT AND ANNA P. M. MICHEL*

Department of Applied Ocean Physics and Engineering, Woods Hole Oceanographic Institution, 266 Woods Hole Rd., Woods Hole, Massachusetts 02543, USA
**Corresponding author: amichel@whoi.edu*

Received 5 August 2021; revised 8 October 2021; accepted 11 October 2021; posted 14 October 2021 (Doc. ID 439787); published 15 November 2021

Sensors that measure dissolved gases directly are needed for environmental, industrial, and biomedical applications. Here we present a hollow core fiber optic sensor capable of measuring dissolved methane gas in liquids using only nanoliters of sample gas. The sensor is based on an anti-resonant hollow core fiber combined with a permeable capillary membrane inlet that extracts gas from the liquid for analysis. Using a small capillary inlet for gas extraction is only possible due to the small amount of sample gas needed for analysis, and it presents new possibilities for dissolved gas analysis in a simple, robust, and compact sensor configuration. We demonstrate the sensing technique using wavelength modulation spectroscopy and measure methane dissolved in water with a 1σ lower detection limit of 230 ppb, a resolution of 45 ppb, and a response time of ~8 min.

https://doi.org/10.1364/AO.439787

1. INTRODUCTION

The measurement of dissolved gas concentrations is important in a wide variety of industrial, environmental, and biomedical applications. Gases in both the gas phase and dissolved in fluids are commonly measured using absorption spectroscopy due to its advantages of high sensitivity and selectivity [1–4]. However, reaching high sensitivity and low detection limits often requires multi-pass cells or high finesse cavities, which necessitate precision optical and mechanical components that increase size and fabrication complexity [5–8]. Measuring gases in dissolved form also often requires additional components to equilibrate or extract the gas into a headspace prior to analysis [9–13]. Such sizable components are not ideal for field portable or *in situ* sensors for which miniaturization is key. Optical cell miniaturization is also desirable when only a limited amount of sample gas is available because it decreases the amount of gas required for analysis. This can be the case for finite samples retrieved in the field, or when there is only a small amount of liquid available for analysis.

In the past decade, several types of hollow core fibers (HCFs) have gained significant attention for their ability to serve as an alternative optical cell for gas analysis with minimal sample volume. These include hollow core photonic crystal fibers [14–18], anti-resonant HCFs [19–22], and dielectric hollow core waveguides [23–25]. These fibers have the advantage of providing long light/gas interaction lengths with extraordinarily small sample volumes, typically requiring only 2 to 200 nanoliters of gas to fill a 1-meter fiber [26]. As an example, extracting enough atmosphere-equilibrated gas from water to fill the fiber would require degassing only 0.09 to 9 μL of water. These characteristics are particularly advantageous for membrane-based dissolved gas sensors due to the slow nature of gas diffusion across the membrane. Minimizing the amount of gas required for analysis can be key for both miniaturizing the size of the gas inlet as well as decreasing the sensor response time.

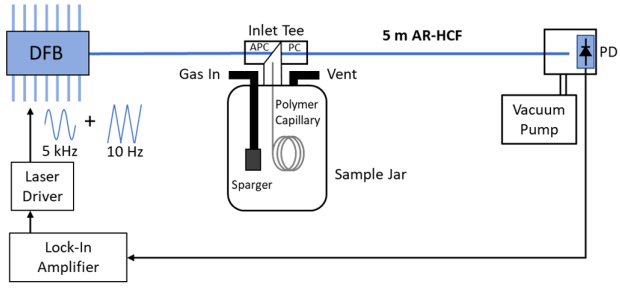

Fig. 1. Diagram of the sensor setup. Blue lines—optical fiber; Black lines—electrical connections. Light from a 1650.9 nm DFB is coupled to a 5 m AR-HCF via an inlet tee. A Teflon AF polymer capillary is also attached to the inlet tee to extract dissolved gas from a solution in a sample jar. The light and the gas exit the AR-HCF in a sealed cell containing a photodiode (PD), and a vacuum pump lowers pressure at the fiber output. A lock-in amplifier provides a laser modulation signal and extracts the 2f signal output. For a dissolved gas measurement, the sample jar is filled with water, and sample gas is bubbled in until equilibrium is reached. A vent on top of the jar allows the sample gas to escape so the pressure in the jar remains at 1 atm.

Here, we utilize a revolver-type [19,27] anti-resonant hollow core fiber (AR-HCF) and 2f wavelength modulation spectroscopy (WMS) to realize a simple and compact sensor for measuring dissolved gases in fluids (Fig. 1). For gas extraction, the sensor employs a gas-permeable polymer capillary membrane inlet, the small size of which is only feasible due to the tiny amount of gas required to fill the fiber, and we demonstrate and characterize the sensor's performance for measuring dissolved methane in water.

2. SENSOR DESIGN

The sensor consists of a 1650.9 nm distributed feedback laser (DFB) (15 mW LD-PD/Ideal Photonics) coupled to a 5 m AR-HCF (iXblue IXF-ARF-45-240) using an FC/APC connector for the laser fiber and an FC/PC connector for the AR-HCF (Fig. 1). This configuration leaves a small ∼85 μm gap between the two fibers through which gas can enter the HCF. The coupling loss for this configuration was typically ∼3 dB, and the minimum bend radius of the fiber is specified as 6 cm. The fiber connection is enclosed in a custom fabricated and sealed "tee" adapter that interfaces to the gas-permeable polymer capillary. The capillary is sealed at its distal end to prevent water from entering. Care was taken in the design to minimize the gas volume inside the tee adapter. Light at the opposite end of the AR-HCF exits into a sealed chamber containing a photodiode used to measure the absorption signal. The sealed chamber is also connected to a vacuum pump which is used to create a pressure differential between the inlet and outlet of HCF. Such a pressure gradient facilitates rapid filling of the fiber [28,29].

The AR-HCF was chosen for its nearly single-mode operation in the near-infrared, where fiber-coupled laser and detector components are both inexpensive and widespread, and for its 46 μm core diameter, which results in a small sample volume that can still be filled within minutes. Though a photonic bandgap fiber could have been used, such fibers typically have much smaller core diameters and thus would have resulted in a significantly longer response time. The operating range of the fiber is 1350–1850 nm, which covers a range of important gases including methane (CH_4), carbon dioxide, carbon monoxide, acetylene, hydrogen sulfide, hydrogen chloride, ammonia, and nitric oxide.

The fiber structure consists of a 46 μm core surrounded by a 99 μm outer diameter (OD) cladding composed of seven longitudinal tubes each ∼12 μm in diameter. The detector is an amplified InGaAs photodiode. The laser was centered on the 1650.96 nm methane absorption transition via current and temperature tuning using a laser driver (Thorlabs ITC4001). A lock-in amplifier (Zurich Instruments HF2LI) was used to both generate a small amplitude 5 kHz sine wave laser current modulation and to acquire the 2f WMS absorption signal with a time constant of 1 ms. The amplitude of the current modulation waveform was adjusted to maximize the magnitude of the 2f signal. The laser was passively held (no feedback) at the center of the methane transition, except for when a 1 Hz large amplitude triangle waveform was occasionally added to record the full absorption feature (as in Fig. 5).

A Teflon AF polymer capillary (508 μm OD × 254 μm inner diameter (ID) × 1 m long) was used to extract the dissolved gas via diffusion across the membrane [30]. This long length ensured the gas inside the capillary was in close equilibrium with the surrounding water before entering the AR-HCF (see Supplement 1). Even though equilibrium is not required for a dissolved gas sensor, it makes sensor calibration and characterization simpler since it significantly reduces the effect of the membrane's selectivity to various gases.

3. RESULTS

To first characterize the sensor's response to methane gas, the capillary membrane inlet was removed from the adapter tee, leaving only a small stem that was inserted into the sample jar. The gas in the jar was then replaced by flowing ultra-zero air (<100 ppb methane) followed by increasing concentrations of methane/air mixtures from 1 ppm to 1,000 ppm. The gas in the jar was always maintained at atmospheric pressure. The 2f signal recorded during the calibration is shown in Fig. 2 (black). Next, a calibration using dissolved gases was performed by reassembling the Teflon tube into the inlet tee and inserting it into the jar. The jar was then filled with tap water which was sparged with ultra-zero air followed by increasing concentrations of methane/air mixtures until equilibrium was reached. During the full experiment, the solution was continuously stirred to avoid diffusion boundary layer effects on the water side of the capillary membrane [13,31]. The 2f signal during the calibration is shown by the blue data in Fig. 2, and the calibration curve in Fig. 3.

After the calibration, the sensor's resolution was studied by inspecting the signal behavior at low methane concentrations. Figure 4 shows the sensor signal converted to dissolved methane concentration during the calibration step from ultra-zero air to 1 ppm. The 1 ppm step is clearly visible, and the standard deviation of the signal during the zero air portion (time 0 to 23 min) is under 70 ppb, indicating resolutions of this magnitude are possible over time scales of tens of minutes.

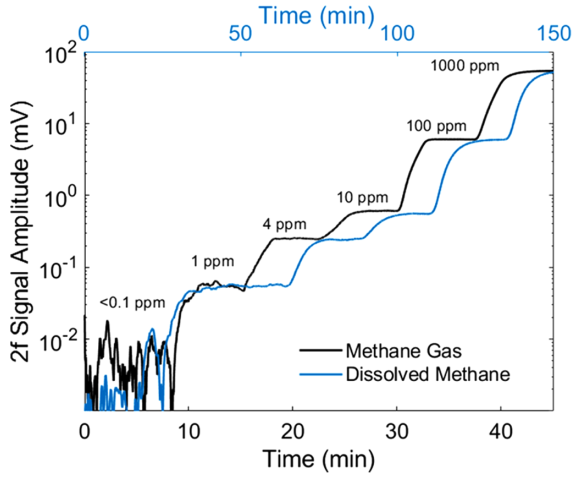

Fig. 2. Time series for two calibrations of methane from 0 ppm to 1000 ppm. The first calibration was obtained by sending methane gas directly into the AR-HCF (black). The second calibration was obtained by measuring dissolved gas extracted through the capillary membrane inlet (blue). Note the longer time scale for the dissolved gas calibration.

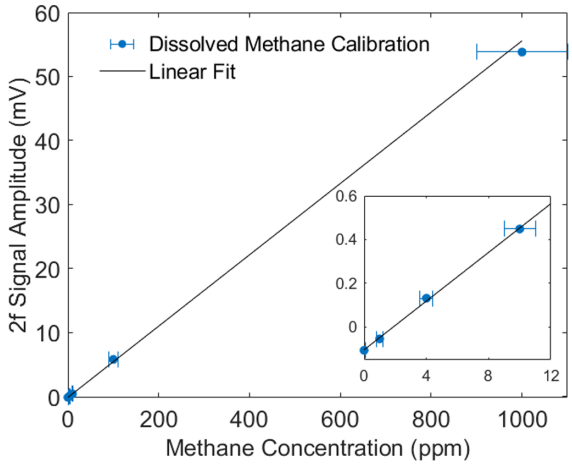

Fig. 3. Calibration for measuring dissolved methane through the membrane inlet. The linear fit was performed using only the first four points for better accuracy at lower concentrations. The inset shows the low concentration values. Error bars indicate the concentration uncertainty for the gas standards used.

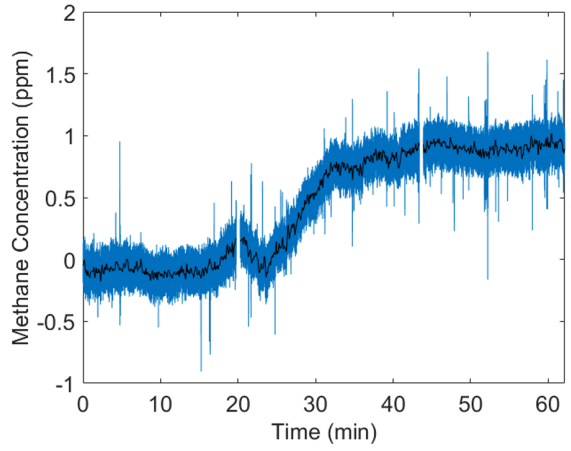

Fig. 4. Sensor respondse to a change from dissolved zero air to 1 ppm dissolved methane. The raw data (blue) and the data with 10 s averaging (black) are shown. The gaps in the data seen at both 20 min and 43 min are periods of time when the full spectrum was scanned as shown in Fig. 5.

To further assess the signal at low concentrations, scans of the full absorption feature were recorded during the calibration for the steps of zero air, 1 ppm CH_4 and 4 ppm CH_4 (Fig. 5, top). The individual scans at these low concentrations show oscillations that continue past the range shown in the figure and are suspected to be interference fringes generated by the laser, the AR-HCF, or the fiber junction in the tee adapter. Nevertheless, these interferences were typically quite stable for durations of minutes to hours, and the zero-air scan could be subtracted from the 1 ppm and 4 ppm scans to more clearly see the methane features (Fig. 5, bottom).

The sensor's detection limit was assessed by equilibrating the sample water with zero air and monitoring the signal over a period of 8 h (Fig. 6). An Allan deviation analysis was used to determine the performance over various time scales. The result agrees well with the performance described above in that

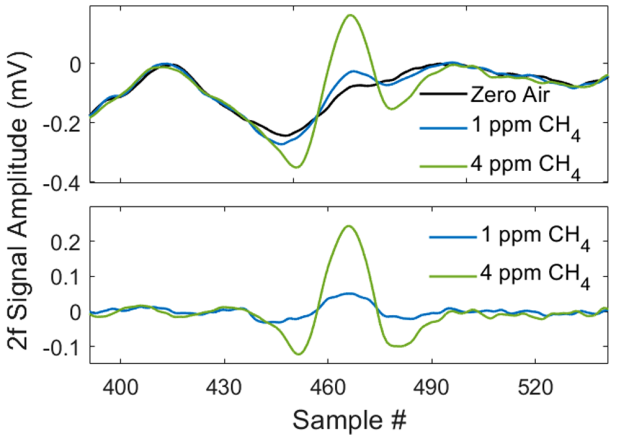

Fig. 5. Absorption features recorded by scanning the center wavelength of the laser across the methane transition for dissolved gas concentrations of zero air, 1 ppm CH_4 and 4 ppm CH_4 (top). The scans for 1 ppm and 4 ppm were subtracted from the zero-air scan to more clearly see the methane feature (bottom).

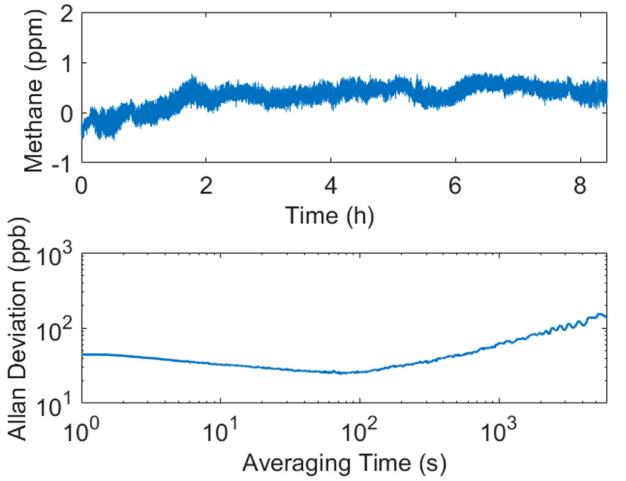

Fig. 6. Stability data and Allan deviation of the sensor signal acquired while monitoring dissolved zero air.

changes below 100 ppb are resolvable over time scales of seconds to minutes, reaching a minimum of 25 ppb for an averaging time of ~100 s. However, long-term drift becomes the predominant feature affecting performance for time scales longer than ten minutes, and it reaches $\sigma = 230$ ppb over several hours, which we define as the sensor's lower detection limit.

Lastly, the response time of the sensor was characterized by recording the signal when it was immediately subjected to a 1000 ppm step in methane in either gaseous or dissolved form (Fig. 7). The response to a gas phase sample was tested similarly as described previously in that the capillary inlet was removed, and the gas in the jar was quickly flushed with a 1000 ppm methane/air mixture. For dissolved methane, the step response was achieved by pre-equilibrating the water in the jar with 1000 ppm methane, and quickly inserting the capillary inlet into the solution. The T_{90} response time for the gas phase test is 2.1 min, while the T_{90} response time for the dissolved gas test is 8.1 min. The shape of the two curves is also quite different due to the different processes limiting the response time. The gas phase test

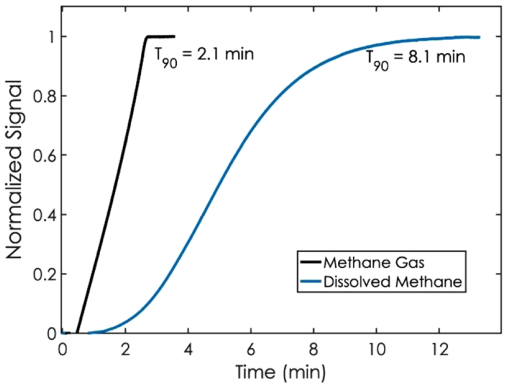

Fig. 7. Response time of the sensor for rapidly flushing the jar with 1000 ppm methane gas with the capillary inlet removed (black) and for measuring dissolved methane extracted through the capillary inlet (blue).

exhibits sharp start and end points, indicative of the sample gas immediately reaching and then filling the fiber. In contrast, the dissolved phase test exhibits a more gradual response which is dominated by the gas concentration reaching equilibrium inside the capillary inlet.

4. DISCUSSION AND CONCLUSIONS

Overall, the work presented here demonstrates the use of hollow core fibers to measure dissolved gas in liquids with a response time of minutes. For this specific sensor configuration, the resolution at the response time of 8.1 min is 45 ppb, and the long-term drift indicates a 1σ detection limit of 230 ppb. Potential methods for mitigating drift include active thermal control of the fiber components, improved laser stabilization, or more elaborate signal processing that uses the full absorption scan.

These results presented here compare favorably to other works that have detected methane using hollow core fibers. For example, previous works in the near infrared using hollow-core photonic bandgap fibers have reached detection limits of between 0.36 ppm and 10 ppm using fiber lengths from 0.45 to 5.1 m [15–17], and other works in the mid-infrared using anti-resonant fibers have reached detection limits between 24 ppb and 500 ppb using ∼1-m-long fibers [22,32]. As with all of these techniques, there are compromises between fiber type, wavelength range, sensitivity, fiber length, bend radius, and response-time.

While absorption spectroscopy is typically known for its high selectivity, the capillary inlet in this setup adds a complication since different gases permeate through the Teflon AF polymer at different rates [33]. For example, the permeability of Teflon AF to nitrogen, oxygen, and carbon dioxide, are respectively 1.4, 2.9, and 8.2 times that of methane. As a result, if those common gases are present in high balance quantities, care must be taken to ensure the gas concentrations inside the polymer capillary are always in full equilibrium with the gas in the water. Otherwise the gas concentrations inside the capillary will vary from that of the sample solution. The required equilibrium can be achieved by ensuring the rate of gas flow through the hollow core fiber is slow enough such that the pressure inside the polymer capillary is able to closely match the total dissolved gas pressure in solution. For the experiments reported here, there is good indication to believe this condition was met for two reasons. First, calculations according to [Supplement 1] indicate the pressure inside the capillary matched the solution gas pressure to within 10%, and second, the similarity between the two calibrations shown in Fig. 2 suggests that the membrane has minimal impact on the sensor's ability to accurately quantify methane. A separate interference consideration is for the effect of water vapor, which permeates through Teflon AF 12.1 times faster than methane, and for which the partial pressure also varies with temperature. Even so, saturated water vapor pressure varies from only ∼0.6% to ∼4% from 0°C to 30°C, indicating the effect of water vapor pressure variations due to temperature should be small. As for how the absorption of these common gases interfere with the absorption signal of methane at 1650.9 nm, oxygen and nitrogen have no effect. Carbon dioxide begins to interfere with 2 ppm levels of methane once it reaches 10% and above, and water vapor begins to interfere at levels of 20% and higher. Despite these positive indications, interferences from other gases should be experimentally tested to confirm these predictions.

The demonstrated sensor has a range of potential applications. For example, the inlet capillary can withstand pressures >1000 psi without collapsing, which could enable the measurement of environmental gases in the deep ocean or gases in high pressure industrial fluids. The small diameter of the capillary inlet also enables dissolved gas analysis inside small tubes or when only a limited amount of sample is available for analysis. Such situations might occur in microfluidic systems or when analyzing samples of blood or saliva. While the detection limit and response time as reported offer suitable performance for many situations, in the future, both can be tailored to various applications by adjusting the properties of the capillary inlet or the HCF. For example, our primary motivation for this work was high pressure ocean applications, and thus we selected a thick-walled durable material for the capillary. The capillary length could be reduced for low pressure applications by selecting a different material or wall thickness, or by relaxing the requirement for gas equilibration. By varying these parameters, along with the length of the HCF, one could increase or decrease sensitivity and response time, with various compromises between the two. In addition, combining two or more light sources into one instrument, or utilizing a broadband light source, could allow for multispecies detection. Thus, a wide variety of sensor configurations is possible for many conceivable applications.

Funding. NOAA Ocean Exploration and Research (NA18OAR0110354); Schmidt Marine Technology Partners (G-2004-59353); Woods Hole Oceanographic Institution (Innovative Technology Award).

Disclosures. The authors declare no conflicts of interest.

Data Availability. Data underlying the results presented in this paper are available in Ref. [34].

Supplemental document. See Supplement 1 for supporting content.

REFERENCES

1. J. B. McManus, M. S. Zahniser, D. D. Nelson, J. H. Shorter, S. C. Herndon, D. Jervis, M. Agnese, R. McGovern, T. I. Yacovitch, and J.

R. Roscioli, "Recent progress in laser-based trace gas instruments: performance and noise analysis," Appl. Phys. B **119**, 203–218 (2015).
2. A. P. M. Michel, S. D. Wankel, J. Kapit, Z. Sandwith, and P. R. Girguis, "In situ carbon isotopic exploration of an active submarine volcano," Deep Sea Res. II **150**, 57–66 (2018).
3. I. Galli, S. Bartalini, S. Borri, P. Cancio, D. Mazzotti, P. De Natale, and G. Giusfredi, "Molecular gas sensing below parts per trillion: radiocarbon-dioxide optical detection," Phys. Rev. Lett. **107**, 270802 (2011).
4. G. Ma, S. Zhao, J. Jiang, H. Song, C. Li, Y. Luo, and H. Wu, "Tracing acetylene dissolved in transformer oil by tunable diode laser absorption spectrum," Sci. Rep. **7**, 14961 (2017).
5. J. B. Paul, L. Lapson, and J. G. Anderson, "Ultrasensitive absorption spectroscopy with a high-finesse optical cavity and off-axis alignment," Appl. Opt. **40**, 4904–4910 (2001).
6. K. Liu, L. Wang, T. Tan, G. Wang, W. Zhang, W. Chen, and X. Gao, "Highly sensitive detection of methane by near-infrared laser absorption spectroscopy using a compact dense-pattern multipass cell," Sens. Actuators B **220**, 1000–1005 (2015).
7. D. A. Long, A. Cygan, R. D. van Zee, M. Okumura, C. E. Miller, D. Lisak, and J. T. Hodges, "Frequency-stabilized cavity ring-down spectroscopy," Chem. Phys. Lett. **536**, 1–8 (2012).
8. R. Grilli, J. Triest, J. Chappellaz, M. Calzas, T. Desbois, P. Jansson, C. Guillerm, B. Ferré, L. Lechevallier, V. Ledoux, and D. Romanini, "SUB-OCEAN: subsea dissolved methane measurements using an embedded laser spectrometer technology," Environ. Sci. Technol. **52**, 10543–10551 (2018).
9. M. Becker, N. Andersen, B. Fiedler, P. Fietzek, A. Körtzinger, T. Steinhoff, and G. Friedrichs, "Using cavity ringdown spectroscopy for continuous monitoring of $\delta^{13}C$ (CO_2) and fCO_2 in the surface ocean," Limnol. Oceanogr. Methods **10**, 752–766 (2012).
10. R. Arruda, D. Atamanchuk, M. Cronin, T. Steinhoff, and D. W. R. Wallace, "At-sea intercomparison of three underway p CO_2 systems," Limnol. Oceanogr. Methods **18**, 63–76 (2020).
11. Y. Li, L. Zhan, J. Zhang, and L. Chen, "Equilibrator-based measurements of dissolved methane in the surface ocean using an integrated cavity output laser absorption spectrometer," Acta Oceanol. Sin. **34**, 34–41 (2015).
12. S. Xiao, L. Liu, W. Wang, A. Lorke, J. Woodhouse, and H. P. Grossart, "A fast-response automated gas equilibrator (FaRAGE) for continuous in situ measurement of CH_4 and CO_2 dissolved in water," Hydrol. Earth Syst. Sci. **24**, 3871–3880 (2020).
13. P. Fietzek, B. Fiedler, T. Steinhoff, and A. Körtzinger, "In situ quality assessment of a novel underwater p CO_2 sensor based on membrane equilibration and NDIR spectrometry," J. Atmos. Ocean. Technol. **31**, 181–196 (2014).
14. F. Benabid, F. Couny, J. C. Knight, T. A. Birks, and P. St.J. Russell, "Compact, stable and efficient all-fibre gas cells using hollow-core photonic crystal fibres," Nature **434**, 488–491 (2005).
15. A. M. Cubillas, M. Silva-Lopez, J. M. Lazaro, O. M. Conde, M. N. Petrovich, and J. M. Lopez-Higuera, "Methane detection at 1670-nm band using a hollow-core photonic bandgap fiber and a multiline algorithm," Opt. Express **15**, 17570–17576 (2007).
16. Q. He, P. Dang, Z. Liu, C. Zheng, and Y. Wang, "TDLAS–WMS based near-infrared methane sensor system using hollow-core photonic crystal fiber as gas-chamber," Opt. Quantum Electron. **49**, 115 (2017).
17. L. Hu, C. Zheng, D. Yao, D. Yu, Z. Liu, J. Zheng, Y. Wang, and F. K. Tittel, "A hollow-core photonic band-gap fiber based methane sensor system capable of reduced mode interference noise," Infrared Phys. Technol. **97**, 101–107 (2019).
18. B. Debord, F. Amrani, L. Vincetti, F. Gérôme, and F. Benabid, "Hollow-core fiber technology: the rising of "gas photonics"," Fibers **7**, 16 (2019).
19. W. Belardi and J. C. Knight, "Hollow antiresonant fibers with low bending loss," Opt. Express **22**, 10091–10096 (2014).
20. W. Belardi, "Design and properties of hollow antiresonant fibers for the visible and near infrared spectral range," J. Lightwave Technol. **33**, 4497–4503 (2015).
21. M. Nikodem, G. Gomółka, M. Klimczak, D. Pysz, and R. Buczyński, "Laser absorption spectroscopy at 2μm inside revolver-type anti-resonant hollow core fiber," Opt. Express **27**, 14998–15006 (2019).
22. P. Jaworski, P. Kozioł, K. Krzempek, D. Wu, F. Yu, P. Bojęś, G. Dudzik, M. Liao, K. Abramski, and J. Knight, "Antiresonant hollow-core fiber-based dual gas sensor for detection of methane and carbon dioxide in the near-and mid-infrared regions," Sensors **20**, 3813 (2020).
23. J. M. Kriesel, N. Gat, B. E. Bernacki, R. L. Erikson, B. D. Cannon, T. L. Myers, C. M. Bledt, and J. A. Harrington, "Hollow core fiber optics for mid-wave and long-wave infrared spectroscopy," Proc. SPIE **8018**, 80180V (2011).
24. D. Francis, J. Hodgkinson, B. Livingstone, P. Black, and R. P. Tatam, "Low-volume, fast response-time hollow silica waveguide gas cells for mid-IR spectroscopy," Appl. Opt. **55**, 6797–6806 (2016).
25. S.-H. Huang, Y.-J. Huang, and H.-C. Chui, "Trace methane sensor using mid-infrared light emitting diode in hollow-core fiber," Sens. Actuators B **282**, 599–602 (2019).
26. J. M. Kriesel, C. N. Makarem, M. C. Phillips, J. J. Moran, M. L. Coleman, L. E. Christensen, and J. F. Kelly, "Versatile, ultra-low sample volume gas analyzer using a rapid, broad-tuning ECQCL and a hollow fiber gas cell," Proc. SPIE **10210**, 1021003 (2017).
27. W. Ding, Y. Wang, S. Gao, M. Wang, and P. Wang, "Recent progress in low-loss hollow-core anti-resonant fibers and their applications," IEEE J. Sel. Top. Quantum Electron. **26**, 1–12 (2020).
28. R. M. Wynne, B. Barabadi, K. J. Creedon, and A. Ortega, "Sub-minute response time of a hollow-core photonic bandgap fiber gas sensor," J. Lightwave Technol. **27**, 1590–1596 (2009).
29. V. Parmar and R. Bhatnagar, "Analysis of gas flow dynamics in hollow core photonic crystal fibre based gas cell," Optik **125**, 3204–3208 (2014).
30. I. Pinnau and L. G. Toy, "Gas and vapor transport properties of amorphous perfluorinated copolymer membranes based on 2, 2-bistrifluoromethyl-4, 5-difluoro-1, 3-dioxole/tetrafluoroethylene," J. Membr. Sci. **109**, 125–133 (1996).
31. S. D. Wankel, Y. Huang, M. Gupta, R. Provencal, J. B. Leen, A. Fahrland, C. Vidoudez, and P. R. Girguis, "Characterizing the distribution of methane sources and cycling in the deep sea via in situ stable isotope analysis," Environ. Sci. Technol. **47**, 1478–1486 (2013).
32. M. Nikodem, K. Krzempek, G. Dudzik, and K. Abramski, "Hollow core fiber-assisted absorption spectroscopy of methane at 3.4μm," Opt. Express **26**, 21843–21848 (2018).
33. J. Scheirs, *Modern Fluoropolymers: High Performance Polymers for Diverse Applications* (Wiley, 1997).
34. Marine Biological Laboratory Woods Hole Oceanographic Institution Library, "Hollow core fiber methane sensor," Woods Hole Open Access Server, 2021, https://darchive.mblwhoilibrary.org/handle/1912/27422.